第 27 卷第 12 期 无 机 化 学 学 报 Vol.27 No.12
2011 年 12 月 CHINESE JOURNAL OF INORGANIC CHEMISTRY 2484-2488

Li_2O-Al_2O_3-GeO_2-P_2O_5 微晶玻璃的微观结构和离子电导率

何 坤* 王衍行 祖成奎 刘永华 赵慧峰 韩 滨 陈 江
(中国建筑材料科学研究总院,北京 100024)

摘要: 采用传统熔体冷却法制备了 $Li_{3-x}Al_{2-x}Ge_x(PO_4)_3$($x$=1.1~1.9)体系玻璃,并通过热处理工艺获得了高电导率的微晶玻璃。通过 XRD、TEM 和交流阻抗等测试方法,研究了该系微晶玻璃的物相组成、微观形貌和锂离子电导率。结果表明:该系统微晶玻璃析出导电主晶相为 $LiGe_2(PO_4)_3$,杂质相为 $AlPO_4$ 和 GeO_2。当 x=1.5 时,由于导电主晶相 $LiGe_2(PO_4)_3$ 晶粒充分长大、分布均匀,所制备微晶玻璃的室温锂离子电导率最高(5.72×10^{-4} S·cm^{-1}),可以满足全固态锂离子电池对电解质高室温电导率的要求。

关键词: 固体电解质; 微晶玻璃; 阻抗谱; 电导率
中图分类号: PM191 **文献标识码**: A **文章编号**: 1001-4861(2011)12-2484-05

Microstructure and Ionic Conductivity of Li_2O-Al_2O_3-GeO_2-P_2O_5 Glass-Ceramics

HE Kun* WANG Yan-Hang ZU Cheng-Kui
LIU Yong-Hua ZHAO Hui-Feng HAN Bin CHEN Jiang
(*China Building Materials Academy, Beijing* 100024, *China*)

Abstract: Fast lithium ion conducting glass-ceramics containing $Li_{3-x}Al_{2-x}Ge_x(PO_4)_3$ (x=1.1~1.9) crystalline phase were prepared from Li_2O-Al_2O_3-GeO_2-P_2O_5 glasses. The results indicate that the glass-ceramics are mainly composed of solid solution $LiGe_2(PO_4)_3$ in the whole x range, following by a small quantity of GeO_2 and $AlPO_4$ crystals as the impurity phases. The total ionic conductivity σ_t reaches a maximum value of 5.72×10^{-4} S·cm^{-1} at room temperature in $Li_{1.5}Al_{0.5}Ge_{1.5}(PO_4)_3$ glass-ceramic with homogeneous crystals distribution.

Key words: solid electrolyte; glass-ceramics; impedance spectroscopy; conductivity

0 Introduction

All-solid-state lithium ion batteries are promising power sources for large scale applications because of their high safety, excellent cycling ability and low packing cost compared to common batteries using liquid electrolyte. Among all components in the all-solid-state lithium ion batteries, solid electrolyte such as Li_2O-Al_2O_3-GeO_2-P_2O_5 glass-ceramics with NASICON-type structure is one of the most important components that control the properties of the batteries[1-3]. These lithium ionic conducting glass-ceramics have been obtained successfully by sol-gel method[4-5], the classical powder-sintering route[6-7] and glass-ceramic process[8-10]. Since homogeneous microstructure and high lithium ionic conductivity, the glass-ceramic process has been widely used to fabricate lithium ionic conducting glass-ceramics. Based on the high lithium ionic conductivity and excellent stability with lithium metal, lithium aluminum germanium phosphate (LAGP) glass-ceramics are immensely attractive as electrolyte in lithium ionic battery. Therefore, it is essential to study the chemical composition on crystals′ microstructure and conductivity of LAGP glass-ceramics. The present

收稿日期:2011-06-10。收修改稿日期:2011-07-25。
国家自然科学基金(No.60808024)资助项目。
*通讯联系人。E-mail:cbmahekun@163.com

work reports the processing and characterization of thermal property, crystal phase, microstructure and ionic conductivity of $Li_{3-x}Al_{2-x}Ge_x(PO_4)_3$ (x=1.1~1.9) glass-ceramics.

1 Experimental

The glass-cerami cs with the composition of $Li_{3-x}Al_{2-x}Ge_x(PO_4)_3$ (x=1.1~1.9) were synthesized by conventional melt quenching technique from mixtures of reagent grade Li_2CO_3, Al_2O_3, GeO_2 and $NH_4H_2PO_4$. The aforementioned chemicals were weighed, mixed, and ground for 30 min in an agate mortar. The batch was heated in an alumina crucible at 700 ℃ for 2 h in order to decompose ammonia, carbon dioxide gases and let water vapor out from the starting materials. The mixture was cooled, thoroughly reground and then heated up to 1 450 ℃ and melted at the temperature for 2 h. The melts were poured onto preheated stainless steel plates and pressed into glass flakes between two steel plates. The glasses were immediately transferred in furnace at 500 ℃ for annealing to relieve the thermal stresses. Finally, the samples were cooled naturally.

The differential scanning calorimetry (DSC, Netzsch STA 449C, Waldkraiburg, Germany) was carried out on approximately 5 mg of fine-powdered glass heated up from room temperature to 1 000 ℃ at a heating rate of 10 ℃·min^{-1}. X-ray diffraction (XRD) data were obtained using a D/Max-2200PC diffractometer (monochromated Cu $K\alpha$ radiation, λ=0.154 184 nm, at 40 kV and 40 mA, SC-70 scintillation counter) in the 2θ rangeof 10°~80° at 0.05° increments. The microstructures morphology of the crystal was characterized by field emission scanning electron microscopy (FESEM) model Supra 55VP. The ionic conductivities were determined using impedance spectroscopy (Solartron 2016 impedance analyzer) in the 0.1~10^6 Hz frequency range with voltage amplitude of 500 mV.

2 Results and discussion

Tab le 1 lists the values of glass transition (T_g), crystallization (T_c), and ΔT ($\Delta T=T_c-T_g$) of $Li_{3-x}Al_{2-x}Ge_x(PO_4)_3$ (x=1.1~1.9) glass samples by extrapolating DSC data. It can be seen that the positions of T_g and T_c shift toward high temperature with the increasing x. It is clear that ΔT increases with increasing x from 1.1 to 1.9, suggesting the enhanced thermal stability of the glass.

Table 1　Glass transition (T_g) and crystallization (T_c) temperatures for $Li_{3-x}Al_{2-x}Ge_x(PO_4)_3$ (x=1.1~1.9) glasses system

x	T_g / ℃	T_c / ℃	ΔT / ℃
1.1	527.4	613.3	85.9
1.3	533.2	617.3	84.1
1.5	538.5	625.4	86.9
1.7	544.4	633.6	89.2
1.9	546.1	637.2	91.1

The XRD patterns of glass-ceramics with various GeO_2 contents after being crystallized at 100 ℃ higher than T_c of each specimen for 8 h are shown in Fig.1. The NASICON-type phase of $LiGe_2(PO_4)_3$ is found to be the dominant crystal phase in $Li_{3-x}Al_{2-x}Ge_x(PO_4)_3$ (x=1.1~1.9) glass-ceramics system. This means that variation in contents of GeO_2 makes a bit of difference on the precipitated crystals of the $Li_{3-x}Al_{2-x}Ge_x$ $(PO_4)_3$ (x=1.1~1.9) glass-ceramics system. Additionally, it is interesting to note that the peak intensity of the major phase $LiGe_2(PO_4)_3$ increases with increasing x, illustrating that GeO_2 makes the as-prepare glass easier to seed out the $LiGe_2(PO_4)_3$ crystal. The peak intensity of the GeO_2 phase increases when $x \geqslant 1.3$. The $AlPO_4$ phase can be observed only when x=1.1 and 1.3, since the Al^{3+} ions are sufficient in these two samples. It is considered that both of the electrically insulating phases, GeO_2 and $AlPO_4$, are concentrated in the grain boundary region.

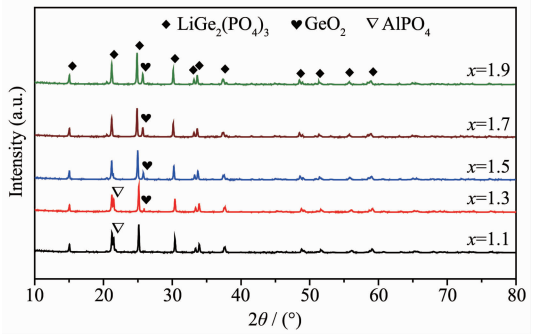

Fig.1　XRD patterns for $Li_{3-x}Al_{2-x}Ge_x(PO_4)_3$ (x=1.1~1.9) glass-ceramics treated at 100 ℃ higher than T_c of each specimen for 8 h

The typical FESEM images of $Li_{3-x}Al_{2-x}Ge_x(PO_4)_3$ (x =1.1 ~1.9) glass-ceramics crystallized at 100 ℃ higher than T_c of each specimen for 8 h are shown in Fig.2. As shown in Fig.2 (a), few grains could be observed in the $Li_{1.7}Al_{0.7}Ge_{1.3}$ $(PO_4)_3$ sample due to low content of GeO_2. Interesting microstructure changes were observed in $Li_{1.5}Al_{0.5}Ge_{1.5}(PO_4)_3$ and $Li_{1.3}Al_{0.3}Ge_{1.7}(PO_4)_3$ glass-ceramics in Fig.2(b) and Fig.2 (c). With an average particle size of 100 nm, the homogeneous microstructures of LAGP glass-ceramics indicate that sufficient content of GeO_2 promotes the growth of particles during crystallization process. However, lesser particles can be observed in $Li_{1.1}Al_{0.1}Ge_{1.9}(PO_4)_3$ glass-ceramic (Fig.2(d)), since most of the particles change into glassy phase with increasing content of germanium oxide. These FESEM observations illustrate that the content of GeO_2 should be 1.5 to 1.7 in $Li_{3-x}Al_{2-x}Ge_x(PO_4)_3$ (x=1.1~1.9) glass-ceramics in order to achieve homogeneous microstructures and uniform distribution of the particles.

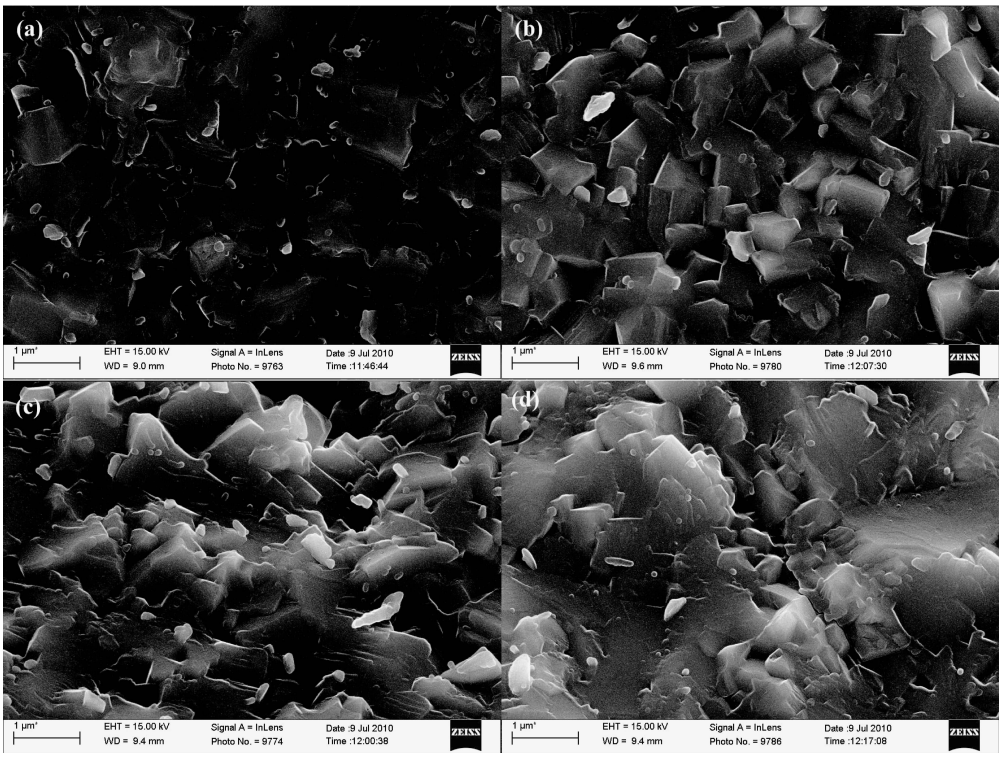

(a) x=1.3, (b) x=1.5, (c) x=1.7, (d) x=1.9

Fig.2 Fracture surface for $Li_{3-x}Al_{2-x}Ge_x(PO_4)_3$ (x=1.1~1.9) glass-ceramics treated at 100 ℃ higher than T_c of each specimen for 8 h

The room temperature complex impedance plots (Cole-Cole plot) are illustrated in Fig.3 for $Li_{3-x}Al_{2-x}Ge_x$ $(PO_4)_3$ (x =1.1 ~1.9) glass-ceramics treated at 100 ℃ higher than T_c of each specimen for 8 h. Only one semicircle and oblique line are observed for all samples. The semicircle represents grain and grain boundary resistances whose diameter is equal to the resistance of the samples. The appearance of a low frequency oblique line in the case of ironically blocking electrodes is an indication of the ionic nature of the NASICON-type material[11-12]. The total resistance R_t of the samples was obtained from the right intercept of the semicircle with the real axis in the plots. And, the total conductivity (σ_t) of LAGP glass-ceramics is calculated by $\sigma_t=H/(S\cdot R_t)$, where H is the sample′s thickness and S is the sample′s surface area.

Li^+ moved from one site to another through the bottlenecks of $[Ge_2P_3O_{12}]^-$ skeleton in LAGP glass-ceramics. So, the particles distribution, microstructures and conductivities of LAGP glass-ceramics are affected by the content of GeO_2. The R_t obviously reduces when x increases from 1.1 to 1.5, and then increases

gradually with further increasing of x, due to the formation of more glassy phase.

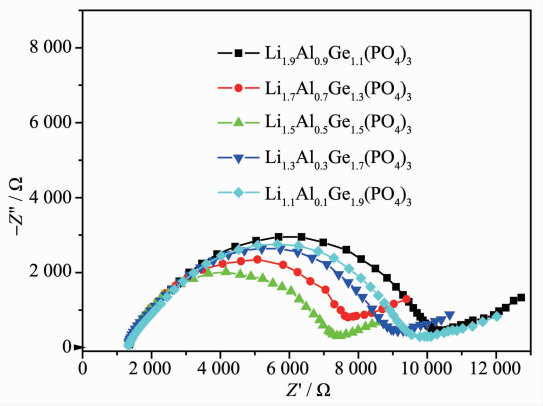

Fig.3　Complex impedance plots at room temperature for $Li_{3-x}Al_{2-x}Ge_x(PO_4)_3$ (x=1.1~1.9) glass-ceramics treated at 100 ℃ higher than T_c of each specimen for 8 h

Fig.4 shows the temperature dependence of the conductivity of $Li_{1.5}Al_{0.5}Ge_{1.5}(PO_4)_3$ glass-ceramic. The conductivity data fit the equation of $\sigma T = A\exp[-E_a/(KT)]$, where A is the pre-exponential term, E_a is the activation energy for conduction and K is the gas constant. Both the conductivity at room temperature and the activation energy are shown in Fig.5. The conductivity increases with the initial increase in x, reaches a maximum value 5.72×10^{-4} S·cm^{-1} at around x=1.5 and then decreases gradually, attributed to the large particles size and negligible particles boundary in Fig.2. All of the $Li_{3-x}Al_{2-x}Ge_x(PO_4)_3$ (x=1.1~1.9) samples exhibit conduc-tivities over 10^{-4} S·cm^{-1}. On the other hand, the E_a passes through a minimum value of

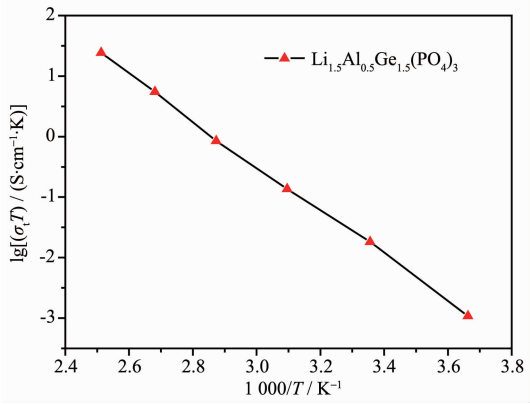

Fig.4　Temperature dependence of the conductivity for $Li_{1.5}Al_{0.5}Ge_{1.5}(PO_4)_3$ glass-ceramic treated at 725 ℃ for 8 h

27.81 kJ·mol^{-1} at x=1.5. And the composition of LAGP glass-ceramics influence on activation energy corresponds to that of conductivity, illustrating that changes in the conductivity are controlled by the changes in the activation energy.

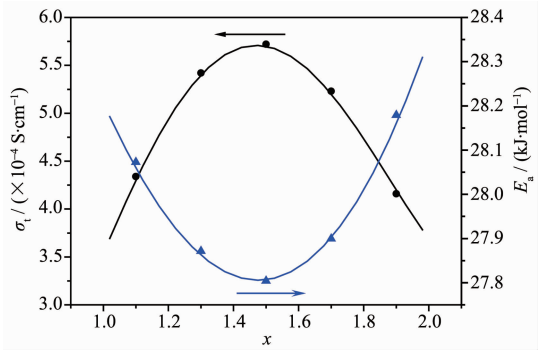

Fig.5　Conductivity and activation energy of $Li_{3-x}Al_{2-x}Ge_x(PO_4)_3$ (x=1.1~1.9) glass-ceramics

Table 2 shows the room temperature total ionic conductivity σ_t of $Li_{1.5}Al_{0.5}Ge_{1.5}(PO_4)_3$ at various crystallization temperature and time. As can be seen, σ_t increases remarkably with the increase in crystallization temperature from 725 ℃ to 825 ℃. The highest conductivity of the LAGP glass-ceramic (5.72×10^{-4} S·cm^{-1}) was obtained for the specimen treated at 825 ℃ for 8 h. However, further increase in crystallization temperature decreases the conductivity. It can also be seen form Table 2 that σ_t increases with the crystallization time from 2 to 8 h, and then lightly decreases with further extension of the crystallization time, suggesting that further extension of crystallization time does not increase conductivity when the particles have fully

Table 2　Total ionic conductivity of $Li_{1.5}Al_{0.5}Ge_{1.5}(PO_4)_3$ at various crystallization temperatures and times at room temperature

Crystallization temperature / ℃	Crystallization time / h	Total ionic conductivity σ_t / (S·cm^{-1})
725	2	3.20×10^{-4}
	8	4.70×10^{-4}
	16	4.60×10^{-4}
825	2	5.12×10^{-4}
	8	5.72×10^{-4}
	16	5.21×10^{-4}
925	2	4.80×10^{-4}
	8	4.60×10^{-4}
	16	4.50×10^{-4}

grown well.

3 Conclusions

Lithium ion conducting glass-ceramics of $Li_{3-x}Al_{2-x}Ge_x(PO_4)_3$ (x=1.1~1.9) were synthesized and characterized. $LiGe_2(PO_4)_3$ is found to be the dominant crystal phase in LAGP glass-ceramics, following by a small quantity of GeO_2 and $AlPO_4$ crystals as their impurity phases. The total ionic conductivity σ_t reaches a maximum value of 5.72×10^{-4} S·cm^{-1} at room temperature in $Li_{1.5}Al_{0.5}Ge_{1.5}(PO_4)_3$ glass-ceramic with homogeneous particles distribution, indicating that LAGP glass-ceramics are promising electrolyte for application in all-solid-state lithium batteries.

References:

[1] Subramanian M A, Subramanian R., Clearfield A. *Solid State Ionics*, **1986**,**18**:562-569

[2] Aono H, Sugimoto E, Sadaoka Y, et al. *J. Electrochem. Soc.*, **1989**,**136**:590-591

[3] Aono H, Sugimoto E, Sadaoka Y, et al. *J. Electrochem. Soc.*, **1990**,**137**:1023-1029

[4] Cretin M, Fabry P J. *Eur. Ceram. So.*, **1999**,**19**:2931-2940

[5] Bohnke O, Ronchetti S, Mazza D, et al. *Solid State Ionics*, **1999**,**122**:127-136

[6] Maldonado M P, Losilla E R, Martinezlara M. *Chem. Mater.*, **2003**,**15**:1879-1885

[7] Thokchom J S, Kumar B. *J. Power Sources*, **2008**,**185**:480-485

[8] Fu J. *Solid State Ionics*, **1997**,**104**:191-194

[9] Li S, Cai J, Lin Z X, et al. *Solid State Ionics*, **1988**,**28**:1265-1270

[10]Thokchom J S, Kumar B. *J. Power Sources*, **2008**,**185**:480-485

[11]Leo C J, Chowdari B V R, Subha Rao G V, et al. *Mater. Res. Bull.*, **2002**,**37**:1419-1430

[12]Xu X X, Wen Z Y, Gu Z H, et al. *Solid State Ionics*, **2004**, **171**:207-213